Intra-envelope four-wave mixing in optical fibers

Eve-Line Bancel, Rosa Santagata, Matteo Conforti, Arnaud Mussot

▶ **To cite this version:**

Eve-Line Bancel, Rosa Santagata, Matteo Conforti, Arnaud Mussot. Intra-envelope four-wave mixing in optical fibers. Optics Express, 2023, 31 (23), pp.37645. 10.1364/OE.501616 . hal-04257428

HAL Id: hal-04257428
https://hal.science/hal-04257428

Submitted on 25 Oct 2023

HAL is a multi-disciplinary open access archive for the deposit and dissemination of scientific research documents, whether they are published or not. The documents may come from teaching and research institutions in France or abroad, or from public or private research centers.

L'archive ouverte pluridisciplinaire **HAL**, est destinée au dépôt et à la diffusion de documents scientifiques de niveau recherche, publiés ou non, émanant des établissements d'enseignement et de recherche français ou étrangers, des laboratoires publics ou privés.

Research Article | Vol. 31, No. 23 / 6 Nov 2023 / Optics Express 37645
Optics EXPRESS

Intra-envelope four-wave mixing in optical fibers

EVE-LINE BANCEL,[1,2,*] ROSA SANTAGATA,[2] MATTEO CONFORTI,[1] AND ARNAUD MUSSOT[1]

[1] Univ. Lille, CNRS, UMR 8523 - PhLAM - Physique des Lasers Atomes et Molécules, F-59000 Lille, France
[2] ONERA, 91120 Palaiseau, France
[*] opex@optica.org

Abstract: We report experimentally on the phenomenon of intra-envelope four-wave mixing (FWM) in optical fibers. We demonstrate that the non-linear interaction between two pulse trains operating at the same repetition rate, but with slightly different carrier frequencies, leads by FWM to the generation of new components within their spectral envelops. The frequency differences between the FWM components and the pump lines are in the RF domain, making it almost impossible to observe the process using a standard optical spectrum analyzer. We show that using a third light source as a multi-line local oscillator makes the analysis of these new spectral components accessible. It enables to extract these FWM components from the spectra of the initial light sources by converting optical frequencies into radio frequencies. The experimental results are in excellent agreement with the numerical simulations.

© 2023 Optica Publishing Group under the terms of the Optica Open Access Publishing Agreement

1. Introduction

Four-wave mixing (FWM) is a fundamental nonlinear effect arising in nonlinear fiber optics when at least two waves interact to generate new spectral components [1]. The efficiency of the process depends on the relative weight between dispersion and non-linearity [2] and can potentially be phase-matched to get a maximum conversion efficiency from the pump to the signal and idler waves [3]. In its simplest form, two continuous wave (CW) lasers generate new side-bands that are symmetrical around them (see Fig. 1(a), CW-FWM). This is also referred to as dual-frequency pumped FWM [4]. The phenomenon can quickly become more complex in long fiber spans, or with higher powers, giving rise to multiple FWM interactions [5]. It leads to broadband spectra made of equally spaced laser lines [6,7]. These light sources known as frequency combs are of great interest for high precision measurements [8]. From a theoretical point of view, this complex non-linear dynamics can be described using a set of coupled equations [5,9–11], valid in the weakly nonlinear regime but also in highly nonlinear ones when energy transfer directions can be reversed [4,5,12]. CW pumps can be replaced by two pulsed pumps, degenerated or not, to get higher peak powers and thus more efficient non-linear interactions. A striking illustration is provided by electro-optic modulator (EOM) combs that are broaden in nonlinear fibers [13,14]. Other configurations based on FWM involving pulsed pump(s) and signals are related to fiber optical parametric amplifiers to amplify or convert signals [15–20] (see Re. [21] for a complete overview). The output spectrum consists of well separated wave-packets, each composed of equally spaced laser lines, for the pump(s), signal and idler waves. This is crucial to ensure that there is no crosstalk between them, to get a high quality of amplification/conversion. This is illustrated in the simplified sketch in Fig. 1(b), showing the general configuration of pulsed-FWM in the degenerate case. We will refer this situation as the (dual-pump) pulsed extra-envelope configuration, because the new sidebands are generated outside the pump envelopes. Note that complex nonlinear effects related to the symmetry breaking induced by a pulsed pump can also be interpreted in terms of FWM [22]. Here too, the new sidebands are generated outside the initial pump spectrum. Thus in all these configurations, referenced by CW-FWM and pulsed-FWM that are illustrated in Figs. 1(a) and (b), the new spectral components generated

#501616 https://doi.org/10.1364/OE.501616
Journal © 2023 Received 28 Jul 2023; revised 19 Sep 2023; accepted 20 Sep 2023; published 24 Oct 2023

Optics EXPRESS

by FWM never overlap with the input CW-pump waves or envelopes. Note that intrachannel FWM interactions had been reported but between adjacent chirped channels in the time domain in dispersion managed systems for telecommunications applications [23]. In this article we study the case of *intra-envelope FWM* process, when the FWM components are generated within the spectral envelope of the input pumps. It occurs when the shift between the pump carrier frequencies is very small compared to their bandwidth and repetition rates (Fig. 1(c)). As an example, we will experimentally implement a configuration with a difference that typically lies in the MHz range. We will show that the FWM interactions between the pulsed pumps lead to the generation of FWM bands within the pump spectrum, with a frequency shift from the pump spectral components in the MHz range. This makes it impossible to observe the new components directly, meaning the process cannot be characterized with standard optical spectrum analysers, and/or the use of highly selective optical filters as in multi-casting [24,25]. We put forward the utilization of a third frequency comb to extract the FWM bands hidden within the optical spectrum. It plays the role of a multi-line local oscillator, as in the context of FWM spectroscopy [26]. This technique enables fast measurements with a high spectral resolution by using a low-bandpass detection setup (photo-diode and oscilloscope), as in dual-comb systems [27,28] which convert optical frequencies into the radio frequency domain.

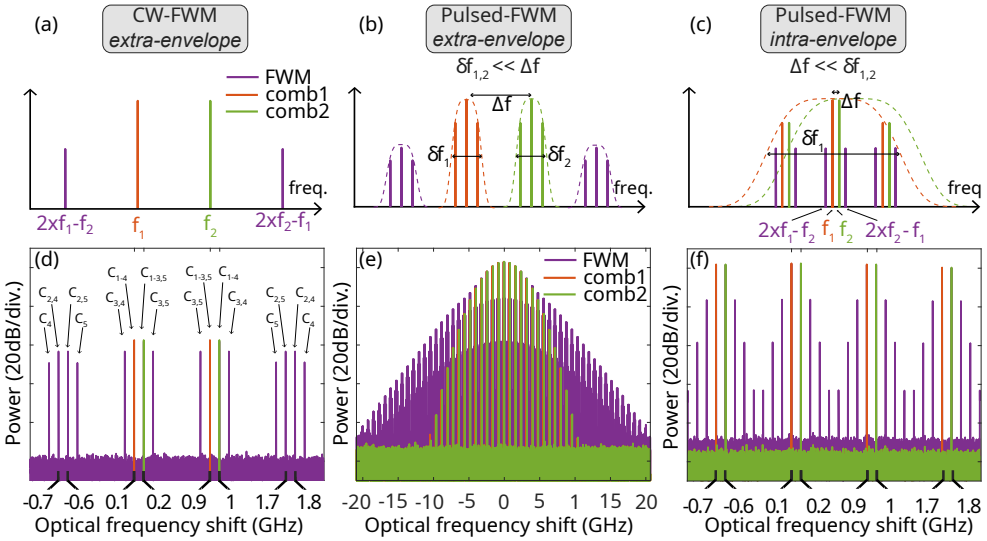

Fig. 1. (a)-(c) Scheme illustrating the different FWM configurations. (a) CW-FWM, (b) pulsed-FWM, extra-envelope case, and (c) pulsed-FWM, intra-envelope case. (d)-(f) Numerics performed by integrating the NLSE. FWM between two frequency combs (d) made of 2 spectral lines, (e) made of 50 spectral lines corresponding to a pulse train of Gaussian with 50 ps pulse duration at FWHM. (f) Zoom on the mFWM packet structure of (e). Parameters : f_{rep}= 800 MHz, $\delta f_{AOM1/2}$= 100 MHz, γ = 1/W/km, β_2 = 1ps^2/km, L= 100 m, and the peak power is 20 W.

2. Intra-envelope FWM

Similarly to the case of extra-envelope FWM process [5,9,10], the dynamics of intra-envelope FWM can turn out to be complex to apprehend. In order to introduce the process, we first describe the most simple configuration with two pulsed pumps, made of only two spectral lines each. They are separated by the repetition rate, which is the same for both pumps: $f_{rep1} = f_{rep2} = f_{rep}$. Let's assume that they also have the same amplitude A. In this simple case, the electric fields are

Optics EXPRESS

respectively written $E_1 = A\left(e^{i2\pi f_1 t} + e^{i2\pi(f_1+f_{rep})t}\right)$ and $E_2 = A\left(e^{i2\pi f_2 t} + e^{i2\pi(f_2+f_{rep})t}\right)$ with $f_{1,2}$, the carrier frequencies of pumps 1 and 2 respectively and $f_2 - f_1 = \delta f_p = \delta f_{AOM1/2}$, their difference. We can calculate the nonlinear interactions between these waves during their propagation in a χ^3 media, such as $E_{FWM} \propto |E_1 + E_2|^2 \cdot (E_1 + E_2)$. It reads as :

$$
\begin{aligned}
E_{FWM} \propto\ & 4A^2(E_1 + E_2) && \} c_1\\
& + 2E_1 \times A^2(e^{i2\pi f_{rep}t} + e^{-i2\pi f_{rep}t}) && \\
& + 2E_2 \times A^2(e^{i2\pi f_{rep}t} + e^{-i2\pi f_{rep}t}) && \} c_2\\
& + 2E_1 \times A^2(e^{i2\pi \delta f_{AOM1/2}t} + e^{-i2\pi \delta f_{AOM1/2}t}) && \\
& + 2E_2 \times A^2(e^{i2\pi \delta f_{AOM1/2}t} + e^{-i2\pi \delta f_{AOM1/2}t}) && \} c_3\\
& + E_1 \times A^2(e^{i2\pi (f_{rep}+\delta f_{AOM1/2})t} + e^{-i2\pi (f_{rep}+\delta f_{AOM1/2})t}) && \\
& + E_2 \times A^2(e^{i2\pi (f_{rep}+\delta f_{AOM1/2})t} + e^{-i2\pi (f_{rep}+\delta f_{AOM1/2})t}) && \} c_4\\
& + E_1 \times A^2(e^{i2\pi (f_{rep}-\delta f_{AOM1/2})t} + e^{-i2\pi (f_{rep}-\delta f_{AOM1/2})t}) && \\
& + E_2 \times A^2(e^{i2\pi (f_{rep}-\delta f_{AOM1/2})t} + e^{-i2\pi (f_{rep}-\delta f_{AOM1/2})t}) && \} c_5
\end{aligned}
\tag{1}
$$

Figure 1(d) shows the modulus square of the spectrum of E_{FWM} calculated numerically by integrating the nonlinear Schrodinger equation (NLSE) [29] in a purely nonlinear fiber (see Fig. 1's caption for parameters). Red and green lines correspond to pumps 1 and 2 (100 MHz & 900 MHz and 200 MHz & 1000 MHz of respective optical frequency shifts) while purple ones correspond to FWM lines. The two first teeth of pumps 1 and 2 (located at 100 & 200 MHz) are separated by $\delta f_{AOM1/2}$ (100 MHz) as well as the second ones (located at 900 and 1000 MHz). The two first teeth of pumps 1 and 2 behave as two CW pumps and generate two side bands on both sides located at 0 and 300 MHz (purple lines), as in the basic CW-FWM configuration (Fig. 1(a)) [29]. A similar mixing occurs between the two second teeth to generate sidebands at 800 and 1.1 GHz. Then two additional wave packets made of 4 new lines generated via multiple FWM interactions centered at −650 MHz and 1750 MHz are generated. All these lines correspond to frequency components that are predicted by Eq. (1), and shown by $c_{i\in[[1;5]]}$ in Fig. 1(d). Note that different combinations of the pump waves frequencies may give rise to the same frequency tooth. This is illustrated in Fig. 1(d). For instance, the tooth located at 1.8 GHz has two contributions. It emerges from the two lines of pump 1 at respectively 0.2 GHz and 1 GHz interacting together, but also from the line 1 GHz of pump 2 interacting with the line at 0.1 GHz of pump 1.

A more realistic configuration involves two pumps composed of several lines, with a similar repetition rate but a slight offset frequency, as represented in Figs. 1(b) and (c). The pumps can be referred as frequency combs. It correspond to the simplified sketch of Fig. 1(c) (pulsed-FWM, intra-pulse). These are two pulse trains of Gaussian pulses of 50 ps at full width at half maximum (FWHM), whose spectra consist of about 50 lines separated of f_{rep} = 800 MHz. We computed the FWM between these two combs by integrating the NLSE [29] in the same fiber used for Fig. 1(d). As it can be seen in Fig. 1(f), each pair of closest comb lines of pumps 1 and 2 behaves as in the basic configuration illustrated in Fig. 1(d). They generate through FWM two new lines on each sides separated by the carrier frequency difference between the combs ($\delta f_{AOM1/2}$= 100 MHz), as in the simple picture of CW-FWM. Harmonics are also generated from these four waves [10] to give birth to wavepackets made of 8 lines for each pair of closest lines of pumps 1 and 2. In addition, multiple FWM (mFWM) processes lead to the generation of new lines outside the initial spectra delimited by the envelops of pumps 1 and 2 as in the basic example illustrated in Fig. 1(d) (see purple packets at −650 and 1750 MHz). To summarize, FWM between two pulsed sources having the same repetition rate f_{rep} but slight different carrier frequencies δf_p leads to the generation of new spectral components mostly generated within the optical spectrum and located at $m\times f_{rep} \pm n\times\delta f_p$ around the carrier frequencies of the pumps with n,m integers. However, the experimental evidence of this phenomenon is challenging because of the small frequency shift between all the generated lines lying in the MHz range, that is by several orders

Optics EXPRESS

of magnitude smaller than the resolution of standard optical spectrum analysers. In the following, we will demonstrate that the use of a third comb playing the role of a multi-lines local oscillator enables to isolate these new spectral components to highlight the intra-envelope FWM process.

3. Evidence of intra-envelope FWM by using a multi-line local oscillator

The idea is based on dual-comb spectroscopy, for which the mixing between one comb and another comb of different repetition rates and carrier frequencies leads to the down conversion of the optical spectrum into the RF domain [27]. The RF spectrum is centered at their carrier frequency difference and it is magnified by a factor equals to the ratio between the repetition rate frequency and the repetition rate difference ($\frac{f_{rep}}{\delta f_{rep}}$). The right choice of these values prevents aliasing by ensuring that the RF spectrum is entirely located within 0 and $f_{rep}/2$ [27]. Here we have two combs, operating at the same repetition rate, and with different carrier frequencies. These pumps will interact in a nonlinear fiber to generate new FWM components, within their input spectral envelops. We mix these combs with a third comb playing the role of the multi-lines local oscillator, as in dual-comb setups. This third comb source has a different repetition rate and carrier frequency compared to combs (pumps) 1 and 2. A simplified sketch illustrated the interactions between the three combs is represented in Fig. 2(a). We kept the same colors as in Fig. 1 for comb 1 and 2 (red and green respectively), and the FWM components (purple) and the third comb is represented in blue. As comb 1(2) and comb 3 have different carrier frequencies, the corresponding RF down converted spectrum is centred at $f_1 - f_3 = \delta \mathrm{f_p} = \delta f_{\mathrm{AOM1/3}}$ ($f_2 - f_3 = \delta \mathrm{f'_p} = \delta f_{\mathrm{AOM2/3}}$), and magnified by $\frac{f_{rep}}{f_{rep} - f_{rep3}}$. This is illustrated in Fig. 2(a), where the RF spectra corresponding to combs 1 and 2 (orange and green respectively) are well separated in the RF domain. About the FWM components, at first order they fulfill the basic FWM relation based on energy conservation which reads as $2f_1 - f_2$ and $2f_2 - f_1$ leading to down converted RF spectra centered at $2\delta f_{\mathrm{AOM2/3}} - \delta f_{\mathrm{AOM1/3}}$ and $2\delta f_{\mathrm{AOM1/3}} - \delta f_{\mathrm{AOM2/3}}$, and magnified by a $\frac{f_{rep}}{f_{rep} - f_{rep3}}$ factor. RF FWM components (purple) are thus isolated from pumps 1 and 2 RF spectra thanks to the down-conversion process. The set-up to generate three coherent pulse trains (combs) is detailed in Fig. 2(b). A continuous-wave laser (NKT Koheras) is amplified and then divided into three channels. It has an ultra-narrow linewidth of 100 Hz. We used a set of EOMs to generate a pulse train of 50 ps duration. Each repetition frequency is adjustable by modifying the radio-frequency signals delivered by arbitrary waveform generators (AWG) that drive the modulators. In channels 1 & 2, we combined a first EOM followed by an EDFA, and then a spectral filter to remove the amplified spontaneous emission in excess. A second EOM is added to increase the extinction ratio (< 50 dB in total). A second EDFA is used in channels 1 and 2 to increase the peak power up to 16 W (650 mW average power) to enhance the FWM efficiency in the fiber. The pulse profile is depicted in Fig. 2(c). We used a fiber of L= 100 m length, with γ = 1/W/km, and β_2 = 1ps^2/km. The repetition rate is $\mathrm{f_{rep}}$ = 800 MHz, and the carrier of comb 1(2) is frequency shifted by using an acousto-optic modulator (AOM1(2), frequency shift of 100 MHz (200 MHz)). In channel 3, a single EOM is used. The repetition rate difference between comb 3 and 1& 2 is $\mathrm{f_{rep}}$ = 1 MHz to get a magnification factor large enough to avoid spectral aliasing in the RF domain after the down-conversion process. All EOMs and AOMs are driven by a set of three arbitrary waveform generators (AWG) that share a common reference at 10 MHz to minimise the timing jitter. We used a low band-pass photo-detector (Thorlabs PDB480C, 5 GHz bandpass) to detect the mixing between the local oscillator (comb 3), combs 1 & 2 and FWM components. The set-up is made of polarisation maintaining fibers from the CW laser to the entry of the fiber where FWM process is generated. Two polarization controllers enables to optimize the beating between the three combs. A −20 dB attenuator is used at the end of the fiber to equalize the powers of the FWM signal and the LO (100 μW) on the photo-detector. The RF signal is low-pass filtered at $\mathrm{f_{rep}}/2$ = 400 MHz using a low-band pass filter.

Optics EXPRESS

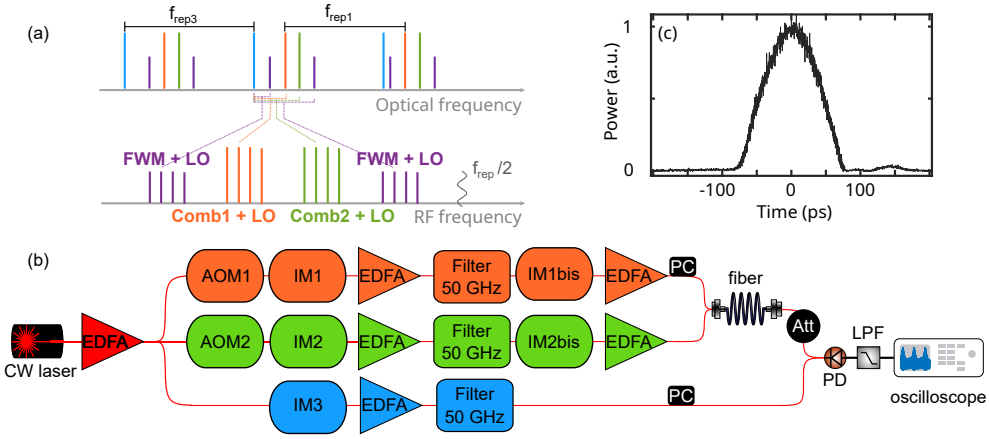

Fig. 2. (a) Schemes of principle. Comb 1 (orange) and Comb 2 (green) at f_{rep1} generate FWM (purple) in a nonlinear fiber. Comb3 (blue) at $f_{rep3} = f_{rep1} + \delta f_{rep}$ down-converts the resulting spectrum in the RF domain. (b) Experimental setup. (c) Pulse recorded at the output of Channel 1. EDFA : erbium-doped fiber amplifier; AOM : acousto-optic modulator; IM : intensity modulator; PC : polarization controller ; LPF : low-bandpass filter; Att : attenuator.

4. Experimental results

We recorded 800 interferograms on the oscilloscope at a sampling frequency F_S = 5 GHz and performed an averaging to increase the signal to noise ratio [27] (see an example of interferogram in Fig. 3(a)). It shows a periodicity equals to the inverse of the frequency difference δf_{rep} = 1 MHz between combs 3 and 1&2. In Fig. 3(a), a zoom on a peak of the interferogram depicts the temporal scanning by the local oscillator. By calculating the Fourier transform of the interferogram, we obtained the down-converted spectrum (Fig. 3(d)). As expected, each packet is centered at its RF frequency offset with the LO: at 100 MHz, the linear beat between the LO and comb1; at 200 MHz, the linear beat between the LO and comb2; at 0 MHz, the beat between the LO and the low frequencies of the FWM; at 300 MHz, the beat between the LO and the high frequencies of the FWM. Thus, the use of a multi-lines local oscillator indeed enables to extract and isolate in the RF spectrum the FWM components hidden within the optical spectrum. Note that the wave packet located at 400 MHz emerges from the mFWM. These experimental results are in excellent agreement with numerical simulations depicted in Fig. 3(c). From these RF spectra, it is possible to numerically reconstruct the optical spectra. This involves subtracting the center frequency of each packet and stretching the spectrum by the inverse of the magnification factor [27,28]. This leads to the optical spectra centered at 193.4 THz in Fig. 3(f) and (h). They have a sinc shape like. We can clearly see combs 1 and 2 (orange and green respectively), having the same repetition rate (800 MHz) and a slightly different carrier frequency (100 MHz). The FWM bands are located on both sides of each closest lines pairs (purple), as expected, and illustrated in the simplified sketch in Fig. 1(c). The reconstructed optical spectra, showing the FWM component interleaved within the optical spectrum, are in excellent agreement with numerical simulations shown in Fig. 3(e) and (g). The only significative discrepancy is the emergence of the second-order FWM sideband at high frequencies in the numerical simulations. We attribute it to the lower signal to noise ratio in experiments which hide these weak sidebands. This agreement confirms the validity of our procedure to reconstruct the optical spectra and highlights the accuracy of our measurements.

Optics EXPRESS

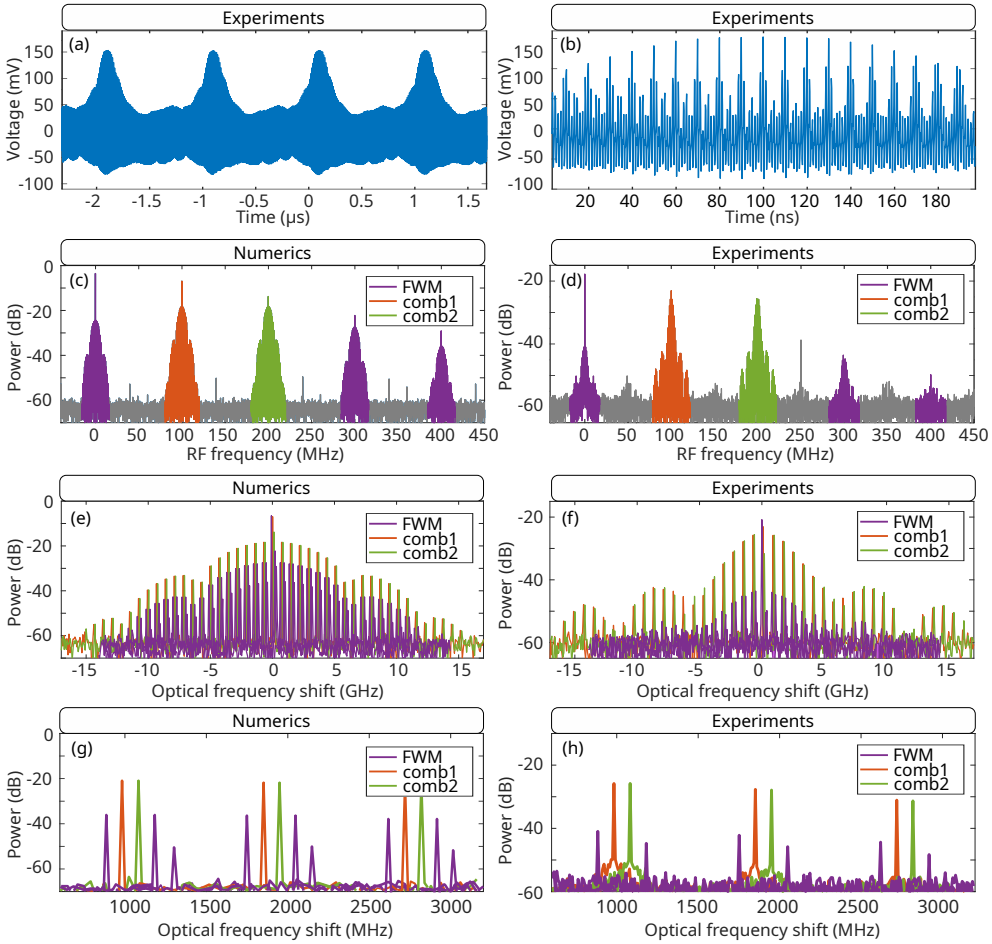

Fig. 3. (a) Recorded interferogram over 4 periods and (b) a zoom. (c) Numerical and (d) experimental RF spectra of the interferogram. (e) Numerical and (f) experimental corresponding optical spectra. (e) Numerical and (f) experimental zoom on the mFWM packet structure of the optical spectrum.

5. Conclusion

In conclusion, we report the first numerical and experimental observation of intra-envelope FWM in optical fibers. We show that two wave packets with almost the same carrier frequency and similar repetition rates can interact nonlinearly to generate new FWM components located within their spectra, and only shifted from RF frequency shifts from the spectral lines of the pumps. We demonstrate the use of a third comb acting as a multi-lines local oscillator to extract and isolate these FWM components in the RF domain. From these measurements, we showed that it is possible to reconstruct the optical spectra, and analyzing the phenomenon with a very good spectral resolution. These observations would not be possible with standard optical spectrum analyzers due to their limited spectral resolution. The very good agreement between experimental and numerical results demonstrates that multi-comb interferometry can be a powerful tool for finely characterizing advanced nonlinear effects in the spectral domain.

Funding. European Regional Development Fund (Photonics for Society P4S); Université de Lille (LAI HOLISTIC); Royal Academy of Engineering (EPSRC Project EP/W002868/1); Centre National de la Recherche Scientifique (IRP

Optics EXPRESS

LAFONI); Conseil Régional Hauts-de-France (GPEG Project); Ministère de l'Enseignement supérieur, de la Recherche et de l'Innovation; Agence Nationale de la Recherche (FARCO, ISITE VERIFICO).

Disclosures. The authors declare that there are no conflicts of interest related to this article.

Data availability. Data underlying the results presented in this paper are not publicly available at this time but may be obtained from the authors upon reasonable request.

References

1. K. O. Hill, D. C. Johnson, B. S. Kawasaki, and R. I. MacDonald, "cw three-wave mixing in single-mode optical fibers," J. Appl. Phys. **49**(10), 5098–5106 (1978).
2. N. Shibata, R. Braun, and R. Waarts, "Phase-mismatch dependence of efficiency of wave generation through four-wave mixing in a single-mode optical fiber," IEEE J. Quantum Electron. **23**(7), 1205–1210 (1987). Conference Name: IEEE Journal of Quantum Electronics.
3. R. H. Stolen, J. E. Bjorkholm, and A. Ashkin, "Phase-matched three-wave mixing in silica fiber optical waveguides," Appl. Phys. Lett. **24**(7), 308–310 (1974).
4. S. Trillo, S. Wabnitz, and T. A. B. Kennedy, "Nonlinear dynamics of dual-frequency-pumped multiwave mixing in optical fibers," Phys. Rev. A **50**(2), 1732–1747 (1994).
5. J. R. Thompson and R. Roy, "Nonlinear dynamics of multiple four-wave mixing processes in a single-mode fiber," Phys. Rev. A **43**(9), 4987–4996 (1991).
6. Y. H. Li, Y. Y. Zhao, and L. J. Wang, "Demonstration of almost octave-spanning cascaded four-wave mixing in optical microfibers," Opt. Lett. **37**(16), 3441–3443 (2012).
7. Z. Tong, A. O. J. Wiberg, E. Myslivets, B. P. P. Kuo, N. Alic, and S. Radic, "Spectral linewidth preservation in parametric frequency combs seeded by dual pumps," Opt. Express **20**(16), 17610 (2012).
8. T. Fortier and E. Baumann, "20 years of developments in optical frequency comb technology and applications," Commun. Phys. **2**(1), 153 (2019).
9. A. Armaroli and S. Trillo, "Modulational instability due to cross-phase modulation versus multiple four-wave mixing: the normal dispersion regime," J. Opt. Soc. Am. B **31**(3), 551–558 (2014).
10. M. Baillot, T. Chartier, and M. Joindot, "Multiple four-wave mixing in optical fibres," *European Conference on Optical Communication, ECOC* pp. 1–3 (2014).
11. G. Cappellini and S. Trillo, "Third-order three-wave mixing in single-mode fibers: exact solutions and spatial instability effects," J. Opt. Soc. Am. B **8**(4), 824–838 (1991). Publisher: Optica Publishing Group.
12. D. L. Hart, A. F. Judy, R. Roy, and J. W. Beletic, "Dynamical evolution of multiple four-wave-mixing processes in an optical fiber," Phys. Rev. E **57**(4), 4757–4774 (1998).
13. D. R. Carlson, D. D. Hickstein, W. Zhang, A. J. Metcalf, F. Quinlan, S. A. Diddams, and S. B. Papp, "Ultrafast electro-optic light with subcycle control," Science **361**(6409), 1358–1363 (2018). Publisher: American Association for the Advancement of Science Section: Report.
14. A. Parriaux, K. Hammani, and G. Millot, "Electro-optic frequency combs," Adv. Opt. Photonics **12**(1), 223–287 (2020). Publisher: Optical Society of America.
15. T. Yamamoto and M. Nakazawa, "Active optical pulse compression with a gain of 29.0 dB by using four-wave mixing in an optical fiber," IEEE Photonics Technol. Lett. **9**(12), 1595–1597 (1997). Conference Name: IEEE Photonics Technology Letters.
16. G. Kalogerakis, M. Marhic, and L. Kazovsky, "Multiple-wavelength conversion with gain by a high-repetition-rate pulsed-pump fiber OPA," J. Lightwave Technol. **23**(10), 2954–2960 (2005). Conference Name: Journal of Lightwave Technology.
17. R. Salem, M. A. Foster, and A. L. Gaeta, "Application of space–time duality to ultrahigh-speed optical signal processing," Adv. Opt. Photonics **5**(3), 274–317 (2013). Publisher: Optica Publishing Group.
18. F. S. Yang, M. C. Ho, M. E. Marhic, and L. G. Kazovsky, "Demonstration of two-pump fibre optical parametric amplification," Electron. Lett. **33**(21), 1812–1813 (1997). Publisher: IET Digital Library.
19. M. Lillieholm, M. Galili, L. Grüner-Nielsen, and L. K. Oxenløwe, "Detailed characterization of CW- and pulsed-pump four-wave mixing in highly nonlinear fibers," Opt. Lett. **41**(21), 4887–4890 (2016). Publisher: Optica Publishing Group.
20. A. Mussot, A. Kudlinski, P. B. d'Augéres, and E. Hugonnot, "Amplification of ultra-short optical pulses in a two-pump fiber optical parametric chirped pulse amplifier," Opt. Express **21**(10), 12197–12203 (2013). Publisher: Optica Publishing Group.
21. M. E. Marhic, *Fiber Optical Parametric Amplifiers, Oscillators and Related Devices* (Cambridge University Press, 2007), 1st ed.
22. M. Erkintalo, Y. Q. Xu, S. G. Murdoch, J. M. Dudley, and G. Genty, "Cascaded phase matching and nonlinear symmetry breaking in fiber frequency combs," Phys. Rev. Lett. **109**(22), 223904 (2012).
23. V. Mamyshev and N. A. Mamysheva, "Pulse-overlapped dispersion-managed data transmission and intrachannel four-wave mixing," Opt. Lett. **24**(21), 1454–1456 (1999).
24. C. K. Huynh, Z. Tong, E. Myslivets, A. O. J. Wiberg, J. R. Adleman, S. Zlatanovic, E. W. Jacobs, and S. Radic, "Noise performance of phase-insensitive multicasting in multi-stage parametric mixers," Opt. Express **21**(1), 804–814 (2013). Publisher: Optica Publishing Group.

Optics EXPRESS

25. S. Radic, "Parametric Signal Processing," IEEE J. Sel. Top. Quantum Electron. **18**(2), 670–680 (2012). Conference Name: IEEE Journal of Selected Topics in Quantum Electronics.
26. B. Lomsadze and S. T. Cundiff, "Frequency comb-based four-wave-mixing spectroscopy," Opt. Lett. **42**(12), 2346–2349 (2017). Publisher: Optica Publishing Group.
27. I. Coddington, N. Newbury, and W. Swann, "Dual-comb spectroscopy," Optica **3**(4), 414 (2016).
28. N. Picqué and T. W. Hänsch, "Frequency comb spectroscopy," Nat. Photonics **13**(3), 146–157 (2019).
29. G. P. Agrawal, "Non linear fiber optics," in *Nonlinear Fiber Optics*, (Elsevier, 2013), pp. i–ii.

134.206.250.119 {ts '2023-10-25 03:21:29'}